Journal of Polymer Science

WILEY

JOURNAL OF POLYMER SCIENCE

RESEARCH ARTICLE OPEN ACCESS

Nucleation and Clarification of Polyamides With Supramolecular Additives

Daniel Kremer | Florian Richter | Johannes U. Heigl | Klaus Kreger | Hans-Werner Schmidt

Macromolecular Chemistry and Bavarian Polymer Institute (BPI), University of Bayreuth, Bayreuth, Germany

Correspondence: Hans-Werner Schmidt (hans-werner.schmidt@uni-bayreuth.de)

Received: 24 March 2025 | **Revised:** 23 May 2025 | **Accepted:** 23 May 2025

Funding: This work was supported by BASF; Universitt Bayreuth.

Keywords: Avrami equation | clarifying agents | haze and clarity | isothermal crystallization | nucleating agents | polyamide 6 | supramolecular additives

ABSTRACT

Nucleating and clarifying agents for semicrystalline thermoplastics based on certain supramolecular additives improve dramatically the optical characteristics such as haze and clarity while maintaining the mechanical properties. This is achieved by an in situ formation of finely dispersed nanosized supramolecular objects, which initiate heterogeneous nucleation reducing the crystallite size and inducing a suitable crystal modification. So far, this concept has been successfully implemented mainly for isotactic polypropylene. Here we report for the first time on supramolecular additives capable of efficiently nucleating and clarifying the engineering plastic polyamide 6 (PA6). This class of supramolecular additives consists of a *trans*-1,4-disubstituted cyclohexane core to which two urea units with aliphatic side groups are attached. We show that these bisurea derivatives enable significant nucleation of PA6 at a concentration as low as 0.02 wt.%. A remarkable characteristic is that the supramolecular additives induce the α-phase of PA6 in rapidly processed injection molded samples. Together with the resulting small crystallite size, this leads to significantly improved optical properties. Compared to the neat PA6, the addition of 0.8 wt.% of a distinct additive improves in 1.1-mm thick specimens the clarity from 68% to 97% and reduces the haze from 98% to 19%, resulting in highly transparent samples.

1 | Introduction

Polyamide 6 (PA6) is one of the most important representatives of engineering thermoplastics. The semicrystalline polymer combines several substantial properties, including, among others, high stiffness and strength, high heat distortion temperature, chemical resistance and good abrasion resistance, and electrical properties [1, 2]. Together with its good processability, the broad range of processing, and the effortlessness to tune its properties by additives, PA6 is used in a wide range of applications in the automotive, industrial, electrical, and consumer sectors.

PA6 is highly opaque when processed using rapid and high-throughput techniques such as extrusion or injection molding. In general, the turbidity of semi-crystalline polymer products is, among other things, strongly dependent on the crystal structure, crystallinity, and crystallite size. Light scattering is caused by large and anisotropic structures such as spherulites or other objects, and differences in the refractive indices of the crystalline and the amorphous phase [3, 4]. In this context, PA6 possesses two stable crystalline modifications, the thermodynamically stable monoclinic α form and the pseudohexagonal γ form [5–7]. In the α form, the chains are in the fully extended zig-zag conformation and grouped into planar sheets. The fully extended chains in the planar sheets are antiparallel to each other, which allows hydrogen bonding between the amide moieties. In the γ form, the chains are arranged in a parallel pleated pattern and the amide moieties are tilted out of the chain axis by about 30° [1, 8–11]. This allows the formation of hydrogen bonds between the amide moieties without strain. The two crystal modifications lead to distinct differences in physical

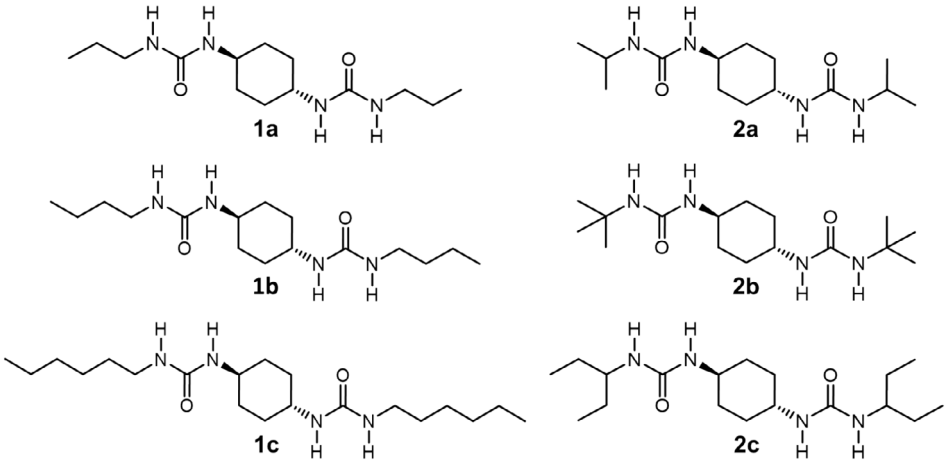

FIGURE 1 | Investigated supramolecular additives for polyamide 6 based on C_2 symmetric bisurea compounds with *trans*-1,4-disubstituted cyclohexane core and linear (1a–c) or branched (2a–c) aliphatic substituents.

and mechanical properties, such as the Young's modulus, which is higher for the α form compared to the γ form [12, 13]. Interestingly, Kolesov et al. have shown that the optical properties of PA6 films can be influenced by the right choice of the crystal structure and crystallite morphology [14]. They demonstrated that PA6 films, which were prepared by cold crystallization, possess the α form of the crystals with a nodular shape and exhibit a high see-through clarity. In comparison, melt-crystallized PA6 films, which possess a spherulitic α form of the crystals, are opaque despite having the same crystallinity. Generally, the thermodynamically stable α form is predominantly achieved by solution casting, annealing at temperatures above 160°C, or slow cooling from the melt. In contrast, the γ form of PA6 is predominantly formed by rapidly cooling from the melt, as is the case in injection molding techniques [1, 11, 15–18]. Thus, to achieve transparent PA6 by rapid processing techniques such as injection molding, it is necessary to induce the α form and to prevent the formation of larger spherulitic-like structures during crystallization. One way to reduce the spherulitic size is to increase the nucleation density. Under a given set of processing conditions, this can be realized by adding nucleating agents. Established nucleating agents for PA6 are talc [19], metallic oxides [20, 21], inorganic metal salts [22, 23], cellulose [24], or CNTs [25, 26]. However, due to potential dispersion issues and agglomeration, they contribute to the light scattering of the incident light. In this context, for the semicrystalline commodity polymer, isotactic polypropylene (i-PP), supramolecular nucleating and clarifying agents based on small molecules are widely used, which circumvent this issue [3, 27–29]. These supramolecular additives rely on the dissolution at elevated temperatures of the building blocks on a molecular level in the polymer melt and the subsequent in situ formation of nano-objects via secondary interactions, that is, hydrogen bonds, upon cooling the melt. Due to the small lateral dimensions of these nano-objects, they do not contribute to the light scattering. Equally important, supramolecular clarifying agents provide an epitaxial surface, which is able to solely induce the α form of i-PP and eventually leads to specimens with excellent transparency [30].

Several prerequisites have to be considered to transfer this concept to polyamides like PA6: The compounds have to be thermally stable above the PA6 processing temperature, have to be soluble in the polyamide melt at specific concentrations, and they have to be capable of interacting with the PA6 via secondary interactions to induce predominantly the nucleation of the α form of PA6. Small molecular building blocks with amide groups are probably too soluble in the PA6 melt, hampering their self-assembly via hydrogen bond formation at elevated temperatures. In contrast, building blocks with urea groups are able to form two hydrogen bonds between the hydrogens of the nitrogen atoms and the carbonyl oxygen, which exceeds the hydrogen bond strength of amides. Such compounds also exhibit good thermal stability [31–33]. Therefore, small molecules that possess two urea groups at a distance from each other, which matches the distance of the two adjacent amide groups within a PA6 chain, should be able to interact with the PA6 chain via hydrogen bonding.

Here, we report on the synthesis and characterization of a largely unknown class of supramolecular additives based on bisurea derivatives capable of nucleating and clarifying PA6. The molecular design of the C2-symmetric bisurea compounds consists of a *trans*-1,4-disubstituted cyclohexane core to which two urea units with peripheral aliphatic side groups are attached (Figure 1). To establish structure–property relationships, we selected short aliphatic side groups with 3 to 6 carbon atoms that are either linear (1a-c) or branched (2a-c). We show that these compounds can be used to efficiently nucleate PA6 and alter the crystallization kinetics. This is achieved by inducing mainly the α form of PA6 crystals. Together with the very small crystallite sizes, this enables the ready fabrication of 1.1-mm thick samples with high transparency under standard processing conditions in injection molding.

2 | Results and Discussion

2.1 | Synthesis and Thermal Properties of Bisurea Compounds

For this study, we designed and synthesized six disubstituted *trans*-1,4-cyclohexane bisurea compounds. Structural variations of the molecular design were performed mainly with respect to short aliphatic substituents, which were linear including

n-propyl, *n*-butyl, and *n*-hexyl side groups or branched including isopropyl, *tert*-butyl, and 3-*pentyl* side groups (Figure 1). This variation allows us to investigate structure–property relationships with respect to the thermal properties of the bisurea derivatives and their nucleation capability upon cooling the polymer melt. The syntheses of the bisurea derivatives were carried out using two different synthesis routes. This includes either the reaction of *trans*-1,4-diaminocyclohexane with corresponding aliphatic isocyanates (1a, 1b, and 2b) or the reaction of *trans*-1,4-cyclohexanediisocyanate with corresponding aliphatic amines (1c, 2a, and 2c). Details of the synthesis route, procedure, and characterization can be found in Sections S1 and S2 of the Supporting Information.

The thermal properties of 1a–c and 2a–c were determined by thermogravimetric analysis (TGA) coupled simultaneously with differential thermal analysis (SDTA, not shown). No melting endotherms were observed for the compounds before the onset of weight loss occurred. For all compounds, the weight loss starts roughly at around 300°C and quickly drops to almost 100% (see Figure S1, ESI). This indicates that sublimation occurs first at higher temperatures, which may be followed by decomposition. The $T_{-5\,wt.\%}$ values for all compounds were above 290°C. For the bisurea compounds with the linear side groups, these values increase with decreasing chain length and were found to be 323°C for 1a, 318°C for 1b, and 292°C for 1c. For the bisurea compounds with branched aliphatic substituents, no clear trend can be found and the $T_{-5\,wt.\%}$ values were found at 303°C for 2a, 315°C for 2b, and 295°C for 2c. These results show that the bisurea compounds feature a sufficiently high thermal stability, which allows them to be used and processed in high-melting point thermoplastics such as PA6, as shown next.

2.2 | Nucleation of Polyamide 6 With Bisurea Compounds

The supramolecular additives were subsequently compounded in PA6 at a processing temperature of 250°C. Visually, the compounded samples do not change color, indicating that no degradation of the additive occurs in the presence of the polymer melt at elevated temperatures. To further demonstrate the thermal stability of an additive in the polymer melt, we compounded PA6 with 0.4 wt.% of a bisurea compound with linear aliphatic side groups and performed 13 heating and cooling cycles with differential scanning calorimetry (DSC) (data not shown). We found that the peak crystallization temperatures ($T_{c,p}$) of the first and second cooling scans are the same, and after 13 cycles, the $T_{c,p}$ decreased by only 0.8°C from 191.9°C to 191.1°C, showing very good stability under repeated thermal stress. Therefore, we evaluated the second cooling scans in further studies. To subsequently investigate how the supramolecular additives nucleate and influence the crystallization temperatures of PA6, we prepared a concentration series in the range of 0.02–1.5 wt.% for each bisurea compound. In a first series of experiments, we evaluated the peak crystallization temperatures ($T_{c,p}$), which were determined by DSC on the second cooling curves after erasing the thermal history by a 5-min hold at 250°C. Experiments with neat PA6 were performed in the same manner and used as reference. The results for the PA6 containing 0.02–1.5 wt.% of the bisurea compounds 1a–c and 2a–c are shown in Figure 2. The averaged peak crystallization temperature ($T_{c,p}$) of neat PA6 was found to be 186.5°C and is shown in each graph for comparison. For the bisurea compounds with linear side groups already at a very low concentration of 0.02 wt.%, $T_{c,p}$ values raised significantly to values of 192.0°C for 1a, 191.3°C for 1b, and 191.1°C for 1c. The $T_{c,p}$ values slightly increase with further increasing concentration to about 0.4 wt.%, after which they do not significantly alter. The maximum $T_{c,p}$ for 1a was 194.1°C at 1.5 wt.%, for 1b at 193.0°C at 0.6 wt.%, and for 1c 193.5°C at 1.3 wt.%.

A similar progression was found for the bisurea compounds with branched side groups, which also featured at a low concentration of 0.02 wt.% a significantly increased $T_{c,p}$ of 191.9°C for 2a, 192.2°C for 2b, and 191.2°C for 2c. The maximum $T_{c,p}$ of 193.3°C was found for 2a at 1.3 wt.%, 194.0°C for 2b at 1.0 wt.%, and 192.5°C for 2c at 0.4 wt.%. These findings strongly suggest that all of the six *trans*-1,4-disubstituted cyclohexane bisurea compounds are highly capable of nucleating the crystallization of PA6. To provide a deeper understanding, we studied the crystallization kinetics of PA6 in the presence of the bisurea compounds.

2.3 | Crystallization Kinetics of Polyamide 6

To study the influence of the bisurea compounds on the crystallization kinetics of PA6, we performed isothermal DSC measurements. In the following, we focus on one representative candidate, namely bisurea compound 2b with *tert*-butyl side groups. Isothermal DSC studies were performed using samples of neat PA6 and PA6 with concentrations of 0.02, 0.4, and 1.0 wt.% of 2b. These three concentrations were selected to study the influence at low concentration (0.02 wt.%) and at about its maximum nucleation effect, which levels off in a plateau (0.4 and 1.0 wt.%). All isothermal measurements were performed at temperatures between 199°C and 210°C, which were well above the standard crystallization temperature (see Figure 2). The isothermal crystallization curves of neat PA6 and PA6 with 2b at various crystallization temperatures T_{iso} are depicted in Figure 3. By increasing the isothermal crystallization temperature, the crystallization curves become broader and the maxima of the exotherms shift to higher times, which is caused by a decrease in the crystallization rate in a nucleation controlled process [34, 35]. For instance, the enthalpic minimum for the neat PA6 is about 9.7 min at a T_{iso} of 202°C. At this temperature, the PA6 with 0.02 wt.% of 2b features an enthalpic minimum already at 3.0 min, indicating a significant acceleration of the polymer crystallization. At higher concentrations such as 0.4 wt.% of 2b, the time to reach the enthalpic minimum is still further reduced. At an isothermal temperature of 204°C, the enthalpic minimum is at 2.5 min for 0.4 wt.% and at 4.3 min for the sample with 0.02 wt.% of 2b. This effect becomes less pronounced upon further increasing the concentration of 2b to 1.0 wt.%. These data goes in line with the findings shown earlier for the peak crystallization temperature (see Figure 2), which suggests a nucleation effect by the additive, which is already present at low concentrations, improves with increasing concentration and levels off.

Since the isothermal DSC curves cover the entire crystallization process for the samples, this allows us to evaluate the data with

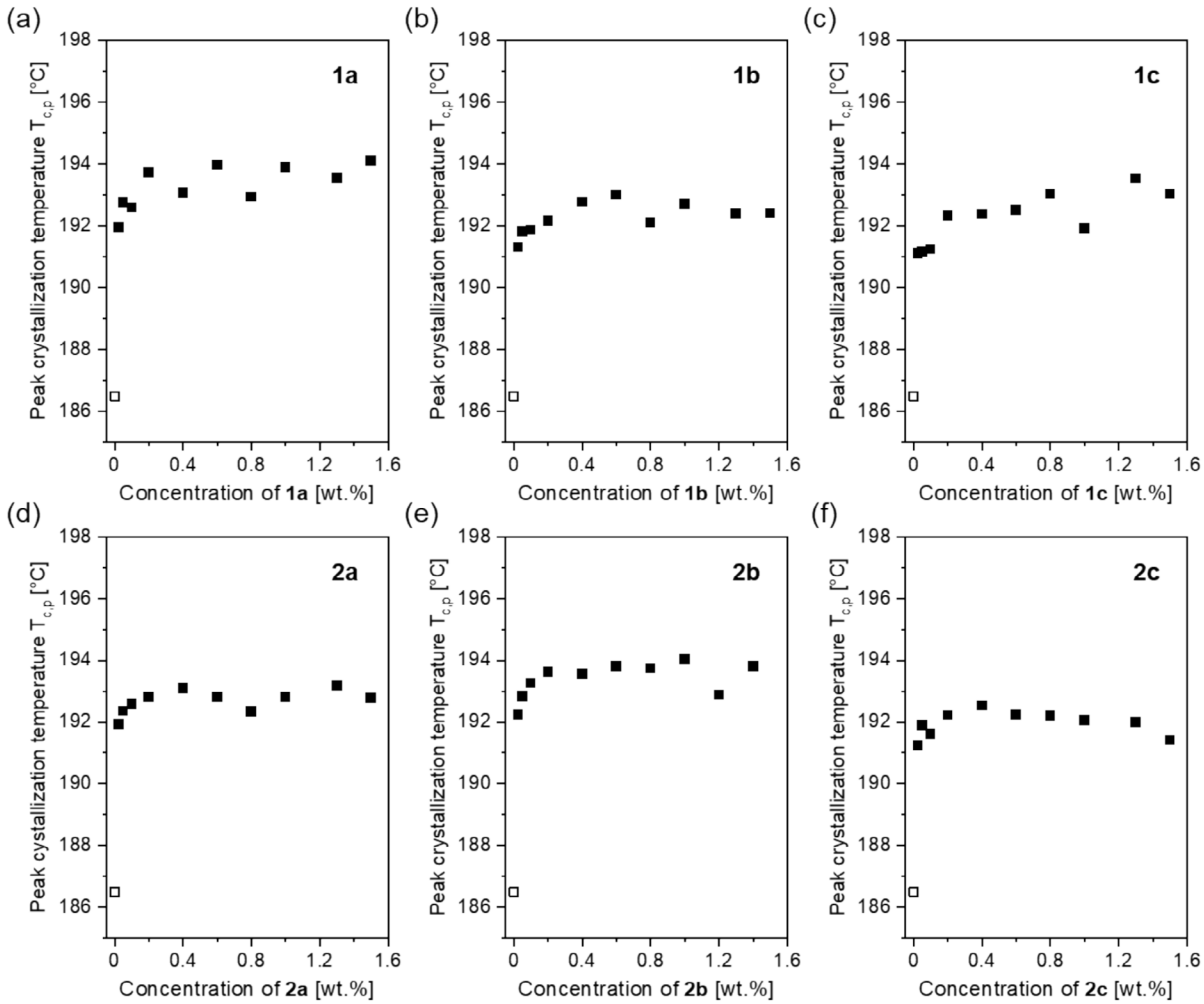

FIGURE 2 | Peak crystallization temperatures ($T_{c,p}$) of neat PA6 (□) and PA6 with different concentrations of bisurea compounds (■). Top row (a–c): Bisurea compounds with linear aliphatic substituents (1a–c). Bottom row (d–f): Bisurea compounds with branched aliphatic substituents (2a–c).

respect to the relative crystallinity $X(t)$ and to apply the Avrami equation. In a first step based on the isothermal data, we determined the relative crystallinity $X(t)$ by integrating the endotherms up to a specific time t and an infinite time t_∞, at which the maximum crystallinity is achieved. The relative crystallinity $X(t)$ can be expressed by Equation (1).

$$X(t) = \frac{X_t}{X_{t,\infty}} = \frac{\int_0^t \frac{dH_c(t)}{dt} dt}{\int_0^{t,\infty} \frac{dH_c(t)}{dt} dt} \quad (1)$$

with dH_c/dt being the heat flow rate.

The relative crystallinities $X(t)$ of neat PA6 and PA6 containing 0.02, 0.4, and 1.0 wt.% of 2b for different isothermal temperatures T_{iso} depending on the time are shown in Figure 4. All curves exhibit the typical sigmoidal shapes. For all samples, the sigmoidal curves shift to higher times by increasing the isothermal temperature T_{iso}.

A characteristic value of isothermal crystallization is the crystallization half-time $t_{0.5}$, which is the time for the sample to reach a relative crystallinity $X(t)$ of 50% at the applied isothermal temperature. Thus, we determined the crystallization half-times $t_{0.5}$ at $X(t)$ of 0.5 for all isothermal temperatures. All data are summarized in Table 1. Comparing the crystallization half-time values $t_{0.5}$ of neat PA6 and PA6 containing 0.02, 0.4, and 1.0 wt.% of 2b at an isothermal temperature of 206°C results in $t_{0.5}$ of 21.3 min for neat PA6, 10.8 min for PA6 with 0.02 wt.% of 2b, 6.5 min for PA6 with 0.4 wt.% of 2b, and 5.3 min for PA6 with 1.0 wt.% of 2b. The $t_{0.5}$ values shift to lower values already at low additive concentration and become more shifted but at a similar level at higher additive concentrations. These findings feature the same trend as shown earlier and show that the addition of 2b increases the crystallization rate, indicating that compound 2b acts as a nucleating agent for PA6.

Based on the relative crystallinity $X(t)$, the Avrami equation can be used to analyze the primary crystallization step. The standard Avrami equation is given by Equation (2), which reads

$$X(t) = 1 - e^{(-Kt^n)} \quad (2)$$

with n being the Avrami index and K the crystallization rate [34, 36–39].

While the value of the Avrami index n depends on the crystal growth geometry and the type of nucleation, the Avrami constant K is influenced by the nucleation density, nucleation

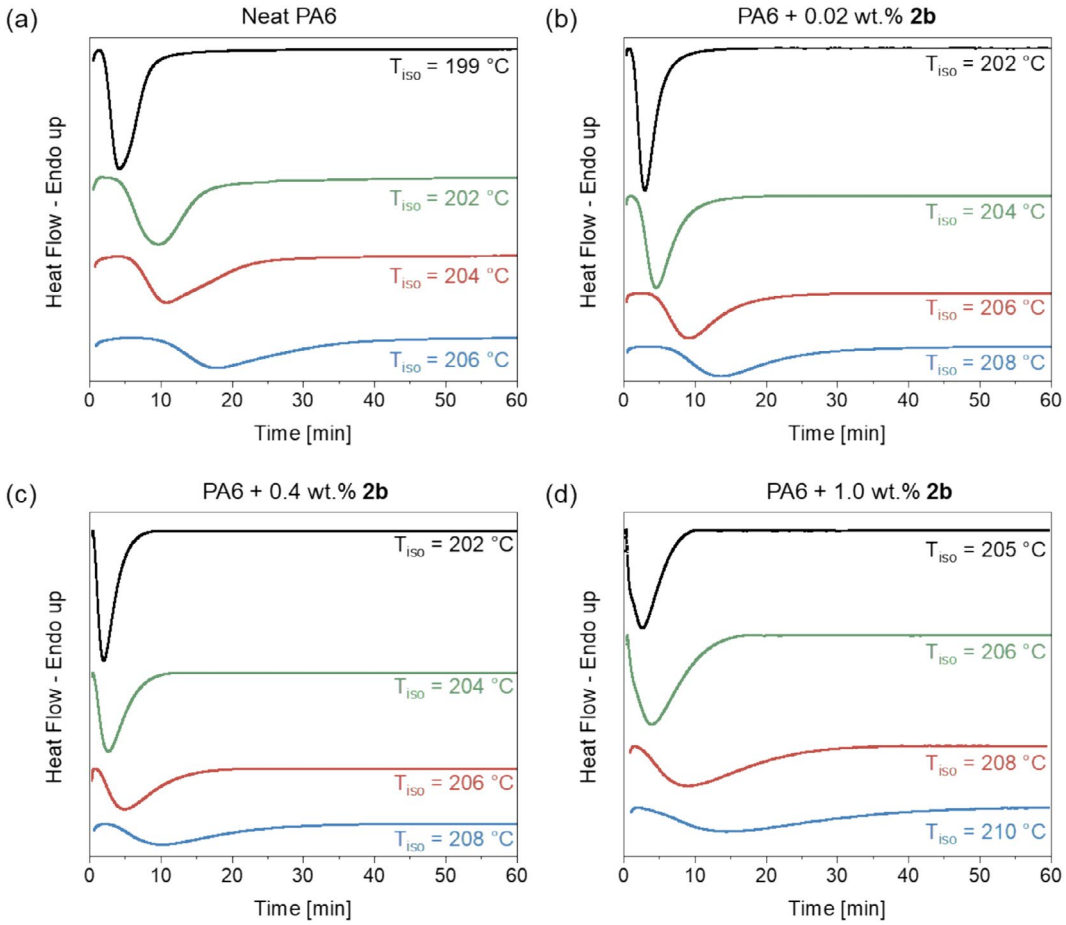

FIGURE 3 | DSC curves of time-dependent polymer crystallization at various isothermal temperatures T_{iso}: (a) neat PA6, (b) PA6 + 0.02 wt.% 2b, (c) PA6 + 0.4 wt.% 2b, (d) PA6 + 1.0 wt.% 2b.

rate, and crystal growth rate. To determine the Avrami index n and the crystallization rate constant K, Equation (2) is typically transformed in its double logarithmic form (Equation (3)), which reads:

$$lg\left[-ln(1-X(t))\right] = n\,lg(t) + lgK \tag{3}$$

Plotting of $\lg[-\ln(1-(X(t))]$ versus $\lg(t)$ allows the determination of the Avrami index n and the crystallization rate constant K by linear regression ($y = mx + c$) with the slope m representing the Avrami index n and the intercept c the crystallization rate constant K. Figure 5 shows the Avrami plots of neat PA6 and PA6 containing 0.02, 0.4, and 1.0 wt.% of 2b at different T_{iso}, including the linear regression. The boundary for the linear regression of $X(t) = 0.05–0.95$ was chosen to exclude predominant secondary processes at the end of the crystallization [39].

The determined values for the Avrami index n and the crystallization rate constant K are summarized in Table 1. The Avrami index n is in the range of 2.97–4.18 for neat PA6, indicating three-dimensional, spherulitic growth from sporadic nuclei. The addition of 0.02 wt.% of 2b narrows the Avrami index n to 2.53–2.92, indicating the appearance of two-dimensional and three-dimensional growth. A further increase of the additive concentration to 0.4 wt.% leads to Avrami indices n of 2.24–2.39 and a concentration of 1.0 wt.% of 2b to n indices between 1.87 and 2.29, which suggests one- to two-dimensional growth [36–39]. Hence, the mechanism of nucleation and growth of crystallites is altered from three-dimensional growth in the case of neat PA6 to one- to two-dimensional growth in the case of PA6 containing compound 2b.

In each dataset for a sample (Table 1), the crystallization rate constant K decreases with increasing T_{iso}, which indicates a decrease in the nucleation and growth rate. However, comparing the K values for neat PA6 and PA6 containing 0.02, 0.4, and 1.0 wt.% of 2b, the K value is strongly increasing with the additive concentration. For instance, the neat PA6 shows a K value of $2.46 \times 10^5\,min^{-n}$ at a T_{iso} of 206°C, which increases to $53.43 \times 10^5\,min^{-n}$ for PA6 with 0.02 wt.% of 2b, to $848.78 \times 10^5\,min^{-n}$ for PA6 with 0.4 wt.% of 2b, and to $3061.25 \times 10^5\,min^{-n}$ for PA6 with 1.0 wt.% of 2b. All compounds of PA with the additive 2b indicate, therefore, a significantly higher nucleus density and nucleation rate [34, 39, 40], which increases with increasing bisurea concentration.

With the knowledge of the crystallization rate constant parameter K and the Avrami index n, this allows one to calculate the crystallization activation energy ΔE_A. Assuming that the isothermal crystallization kinetics of PA6 and PA6 with the bisurea compound 2b are thermally activated, an Arrhenius-type equation can be applied as described by Cebe and Hong [41]. Details are given in Section S4 of the Supporting Information. It was

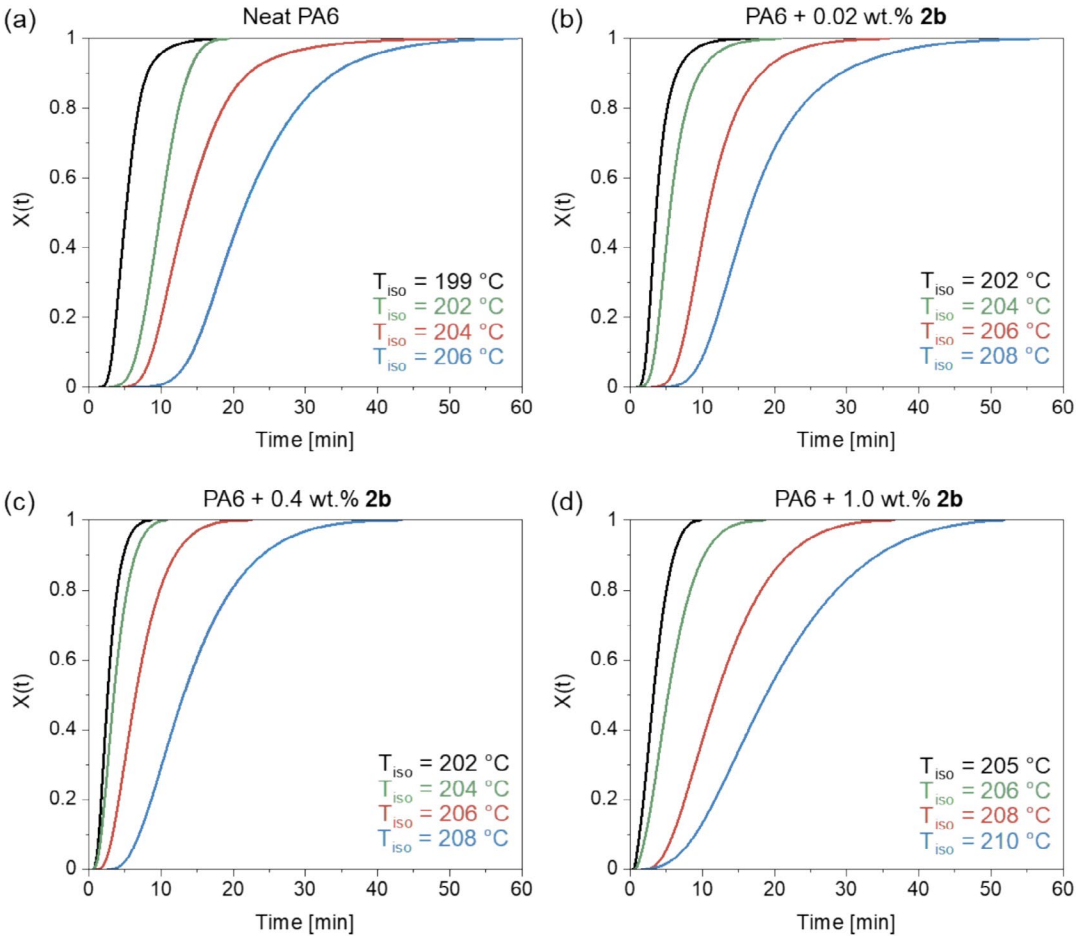

FIGURE 4 | Relative crystallinity $X(t)$ versus the crystallization time of PA6 with and without 2b at different isothermal temperatures T_{iso}: (a) neat PA6, (b) PA6 with 0.02 wt.% of 2b, (c) PA6 with 0.4 wt.% of 2b, (d) PA6 with 1.0 wt.% of 2b.

found that the crystallization activation energy ΔE_A for neat PA6 is −381.8 kJ/mol. The crystallization activation energies ΔE_A for PA6 with 0.02, 0.4, and 1.0 wt.% 2b were calculated to be −497.0, −519.6, and −690.8 kJ/mol, respectively. This represents a significant decrease in the crystallization activation energy in the samples with the bisurea compound compared to neat PA6, which is attributed to a heterogeneous nucleation in the presence of 2b.

All the earlier shown findings such as the peak crystallization temperatures by dynamic DSC and the isothermal crystallization including half-time crystallization as well as Avrami analysis indicated a significant nucleation effect, when the bisurea compound 2b is used. Thus, it can be expected that the crystal morphologies in terms of spherulitic size are varied in the presence of compound 2b. To study the influence of 2b on the spherulitic size, we performed temperature-dependent polarized optical microscopy measurements on the different samples with and without the supramolecular additive. For this, samples were cooled under nitrogen atmosphere from 270°C to 205°C with a cooling rate of 10 K min^{-1} and held at this temperature until the samples were fully crystallized. The optical micrographs for neat PA6 and PA6 with 0.02, 0.4, and 1 wt.% of 2b are shown in Figure S5. It shows that the neat PA6 already crystallizes into small crystallites with sizes in the single-digit micrometer range and no clear spherulitic structure can be seen. Already by adding minute amounts of 2b, that is, 0.02 wt.%, the crystallite size is visibly reduced. This effect becomes apparently more pronounced when the concentration of the bisurea compound 2b is further increased to 0.4 and 1.0 wt.%. This finding provides further evidence for heterogeneous nucleation.

Smaller crystallites are also beneficial to reduce scattering of light and thus improve optical properties such as transparency. Equally important, however, to realize highly transparent specimens is the crystal modification of the semi-crystalline polymer. Thus, we performed wide-angle X-ray scattering measurements on specimens of neat PA6 and PA6 with 0.02, 0.4, and 1 wt.% of 2b.

2.4 | Crystal Modifications of Polyamide 6

Wide-angle X-ray scattering measurements in transmission geometry were performed on various injection molded specimens with a diameter of 25 mm and a thickness of 1.1 mm with and without 2b.

In poorly crystallized polymers such as PA6, the significant superposition of the amorphous halo and the crystalline peaks complicates their separation and ultimately makes it difficult to provide a reasonable number for the crystallinity as

TABLE 1 | Parameters determined by isothermal crystallization of neat PA6 and PA6 containing 0.02, 0.4, and 1.0 wt.% of 2b at different isothermal temperatures T_{iso}. Given are the crystallization half-time $t_{0.5}$, the crystallization rate constant K, the Avrami index n, and the activation energy E_A of the isothermal crystallization.

Sample	T_{iso} (°C)	$t_{0.5}$ (min)[a]	$K \times 10^5$ (min^{-n})[b]	n[b]	E_A (kJ/mol)[c]
PA6	199	5.11	376.79	3.09	−381.8
	202	9.92	4.29	4.18	
	204	13.45	24.75	2.97	
	206	21.27	2.46	3.28	
PA6 + 0.02 wt.% 2b	202	3.58	2228.43	2.53	−497.0
	204	5.48	599.48	2.67	
	206	10.75	53.43	2.92	
	208	16.42	31.02	2.67	
PA6 + 0.4 wt.% 2b	202	2.60	6630.55	2.31	−519.6
	204	3.48	3859.22	2.24	
	206	6.48	848.78	2.29	
	208	13.13	127.61	2.39	
PA6 + 1.0 wt.% 2b	205	3.20	4729.33	2.26	−690.8
	206	5.25	3061.25	1.87	
	208	10.75	210.76	2.29	
	210	18.85	81.64	2.26	

Note: [a]Taken from Figure 4. [b]Determined using Equation (3). [c]Taken from Figure S4 (ESI).

well as the ratios of the α and γ forms [1]. Therefore, we used a method described by Murthy et al., which is based on an amorphous template used in fitting the WAXS pattern [42]. The amorphous template was extracted from a highly crystalline sample with an enriched α phase. The enriched α-phase sample was obtained by melting an injection molded specimen of neat PA6 under vacuum at 240°C for 30 min, subsequent cooling to 205°C, and annealing for 12 h. Proper deconvolution, including the shape and parameters like peak position and full width at half maximum (FWHM), was obtained by subtracting the crystalline peaks from the diffraction pattern. The XRD pattern of the enriched α-phase sample as well as the deconvolution into the crystalline peaks of the α phase and the γ phase as well as the amorphous halo is shown in Figure S6. In the experimental part, Equations (4–8) for the calculation of the partial crystallinities and the ratio of the crystal modification are given. Using the amorphous template of the enriched α phase, the experimental XRD pattern of neat PA6 and PA6 with 1 wt.% of 2b, as well as the deconvoluted crystalline peaks of the α phase and the γ phase and the amorphous halo are shown in Figure 6a,b. The neat PA6 injection molded specimen has a total crystallinity of 30.2% and crystallizes under the given processing conditions into a mixture of the α phase and the γ phase in a ratio of 57/43. Interestingly, the injection molded specimen of PA6 with 1.0 wt.% of 2b leads to the crystallization predominantly in the α phase with an α/γ ratio of 90/10 using the same processing conditions. The total crystallinity is with 31.0% almost the same. In Figure 6c, the XRD pattern of neat PA6 and the PA6 with varying concentrations of 2b from 0.02 to 1.0 wt.% are shown. Already at a low bisurea concentration of 2b of 0.02 wt.%, the α phase is significantly increased to 77.9%. This value increases further with increasing concentration of 2b and finally settles on a plateau with a constant value of about 90%, while the total crystallinity remains largely unaffected. This progression goes well in line with the peak crystallization temperatures shown in Figure 2. All data on the partial α/γ crystallinities and α/γ ratio as well as the total crystallinities are summarized in Table 2.

These findings show that the use of bisurea compound 2b leads not only to the small structural features as shown in polarizing optical microscopy, but also initiate the predominant formation of the α phase of PA6. Both results are a prerequisite for PA6 to allow the preparation of specimens with appealing optical properties.

2.5 | Clarification of Polyamide 6

To study the optical properties, we have prepared injection molded samples with a thickness of 1.1 mm from neat PA6 and PA6 with different concentrations ranging from 0.02 to 1.5 wt.% of all bisurea compounds 1a–c and 2a–c. To characterize the transparency of the objects, the haze and clarity values according to ASTM D-1003 were determined. The haze values refer to the amount of light that is scattered at angles of more than 2.5°. At haze values of 100%, the light is strongly scattered, leading to cloudiness, while at 0% the specimens appear very clear. Clarity refers to the amount of light that is scattered at angles less than 2.5°, with low clarity values of

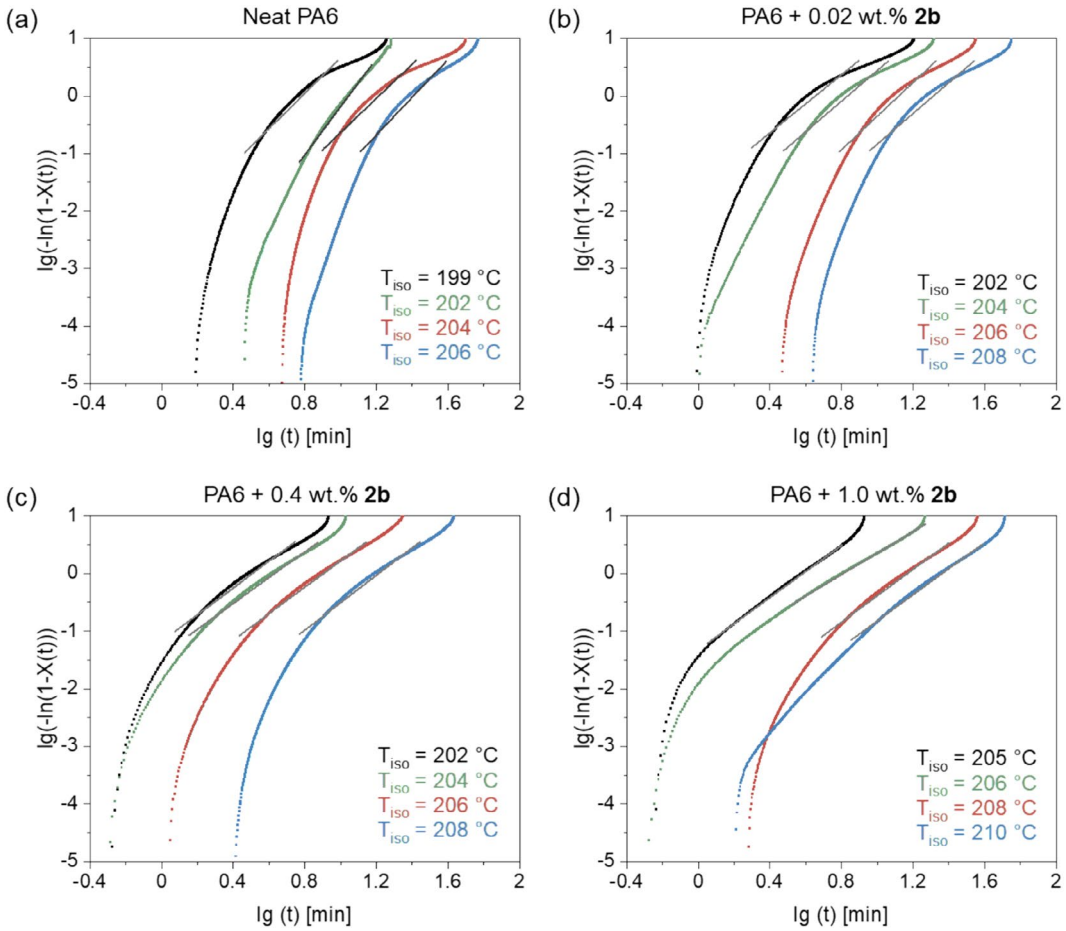

FIGURE 5 | Avrami plots of lg(−ln(1 − $X(t)$)) versus lg (t) of PA6 with and without 2b at different isothermal crystallization temperatures T_{iso}: (a) neat PA6, (b) PA6 with 0.02 wt.% of 2b, (c) PA6 with 0.4 wt.% of 2b, (d) PA6 with 1.0 wt.% of 2b.

0% leading to a loss in sharpness, while values of 100% show excellent clarity.

The haze and clarity values of the different injection molded specimens are shown in Figure 7. The neat PA6 specimen has a haze value of 98.2% and a clarity value of 68.4%. The bisurea compounds with linear aliphatic side groups 1a–c are able to improve the optical properties in the whole investigated concentration range. In particular, the clarity values for all three compounds are well above 90% even at low quantities of the bisurea compounds. The haze values decrease steadily with increasing concentration of bisurea compounds, indicating an improvement in sample transparency. This trend differs from the values for the peak crystallization temperatures, as shown in Figure 2. Within this series, the lowest haze value of 40.6% is achieved with 1a at a concentration of 1.5 wt.%, followed by 50.8% with 1b at a concentration of 1.5 wt.%, and 60.1% with 1c at a concentration of 1.3 wt.%. This indicates that the optical properties improve with increasingly shorter linear aliphatic substituents and that the bisurea compound 1a shows the best performance in both nucleation and clarification of PA6.

A similar trend regarding the optical properties of PA6 is observed for the bisurea compounds with branched side groups 2a–c with increasing additive concentration, yet with some subtle changes. As with bisureas 1a–c, clarity values quickly reach values well above 90%, and haze values improve with increasing concentration for all three compounds. For compound 2a, the best values were determined at a concentration of 1.5 wt.%, with a haze of 36.2% and a clarity of 97.1%. The best values for haze (30.2%) and clarity (96.0%) were found for compound 2c at the same concentration. Within the series from 2a–c, compound 2b shows the most pronounced improvement in optical properties. While clarity increases rapidly with small amounts of the additive 2b, the haze decreases and reaches a plateau at about 0.8 wt.%, where it remains constant in the concentration range investigated. In this concentration range from 0.8 to 1.5 wt.%, we found very low haze values of 19.2%–20.0% and clarity values above 97%. A comparison of both series shows that the branched bisurea compounds 2a–c generally perform better in clarifying PA6 than the linear bisurea compounds 1a–c, despite having comparable $T_{c,p}$ values and thus similar nucleation capabilities. Figure 8 shows the optical appearance of injection molded specimens of neat PA6, PA6 with 0.05 wt.% 2b, and PA6 with 1.0 wt.% 2b, with the latter specimen having an additive concentration that is in the plateau region of haze. The neat PA6 specimen has a pronounced turbid and cloudy appearance. Already at low concentrations of 0.05 wt.% of 2b, the sharpness, which is related to clarity, is significantly improved compared to neat PA6. At a concentration of 1.0 wt.% of 2b, the high transparency of the specimen becomes apparent.

All data clearly show that such bisurea compounds are able to nucleate and clarify PA6. Heterogeneous nucleation is generally attributed to the presence of solid objects in the polymer melt,

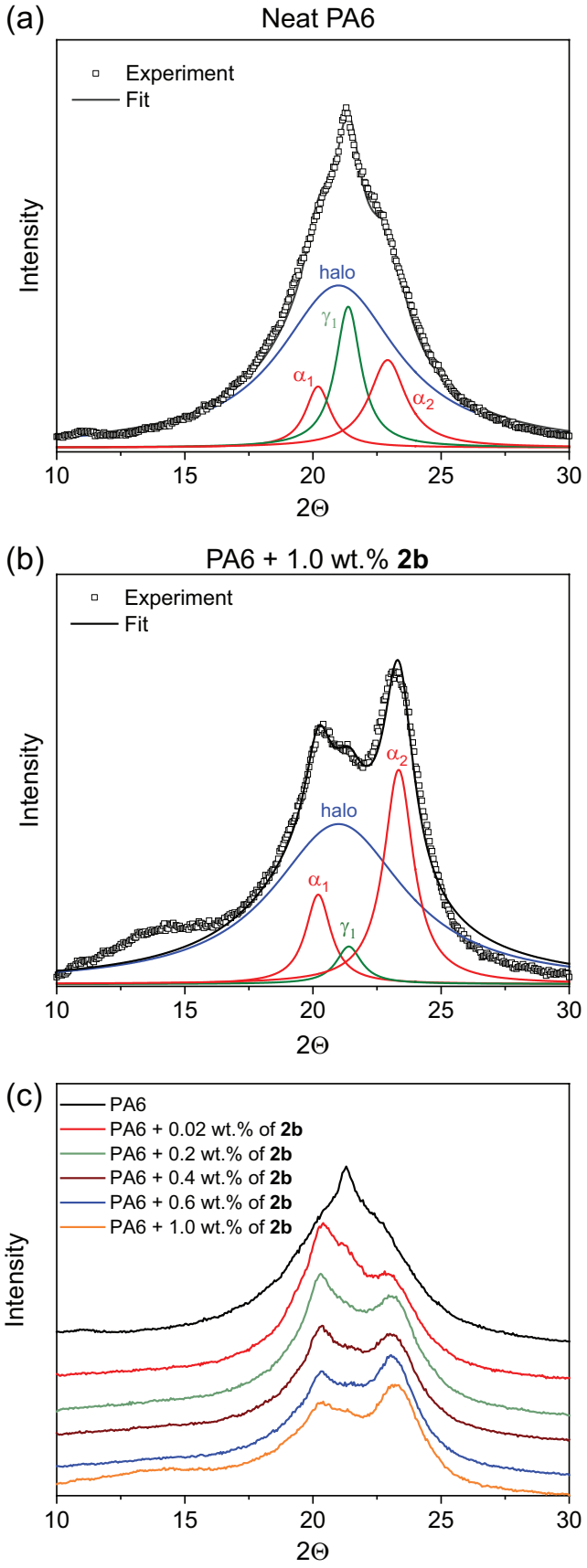

FIGURE 6 | XRD pattern of PA6 with and without 2b. (a) XRD pattern of neat PA6 including experimental data (□), fitted curve (black), and deconvolution into amorphous halo (blue) and crystalline peaks of α_1 (red), α_2 (red), and γ_1 (green); (b) XRD pattern of PA6 containing 1 wt.% of 2b including experimental data (□), fitted curve (black), and deconvolution into amorphous halo (blue) and crystalline peaks of α_1 (red), α_2 (red), and γ_1 (green); (c) XRD patterns of neat PA6 and PA6 with increasing amount of 2b from 0.02 to 1.0 wt.%.

TABLE 2 | Partial crystallinities of the α phase (C_α) and the γ phase (C_γ) and the respective ratios (R_α and R_γ), as well as the total crystallinities (C_{total}) of neat PA6 injection molded specimens and PA6 specimens with varying concentrations of 2b as determined by wide-angle X-ray scattering.

Sample	C_α (%)[a]	C_γ (%)[b]	R_α (%)[c]	R_γ (%)[d]	C_{total} (%)[e]
PA6	17.2	13.0	57.0	43.0	30.2
PA6 + 0.02 wt.% 2b	26.0	7.5	77.9	22.1	33.5
PA6 + 0.2 wt.% 2b	26.0	3.3	88.8	11.2	29.3
PA6 + 0.4 wt.% 2b	26.4	3.4	88.7	11.3	29.8
PA6 + 0.6 wt.% 2b	28.7	3.6	88.9	11.1	32.3
PA6 + 1.0 wt.% 2b	28.0	3.0	90.1	9.9	31.0

Note: Determined using [a]Equation (4), [b]Equation (5), [c]Equation (7), [d]Equation (8), and [e]Equation (6).

providing an epitaxial surface for polymer crystal growth. For the efficient bisurea additive 2b, we have shown that a microcrystalline powder with platelet-like morphology obtained from the polar solvent 2-butanone allows for structure elucidation by NMR crystallographic strategies. 2b exhibits a monoclinic space group P21/c, in which densely packed stacks of 2b are present, driven by strands of hydrogen bonds [43]. Considering the unit cell parameters, it appears that the *a*-axis of 15.4 Å of 2b agrees quite well with the corresponding *b*-axis of 17.2 Å of the α form of PA6 [6]. However, comparing the crystal surfaces of 2b and PA6, as shown in Figure S7, it is evident that this particular 2b polymorph lacks the required epitaxial match for both PA6 polymorphs and is likely unsuitable for nucleation of PA6. On the other hand, a closer look shows that a single stack of 2b results in a very good match of the hydrogen bonds of urea groups with amide groups in the α form of PA6, which cannot be realized for the γ form [5]. This may explain the predominant formation of the α form of PA6 in the presence of bisurea compounds. One possible explanation is therefore that the bisurea compounds self-assemble into another polymorph during compounding, in which such stacks are still present. Further considerations may

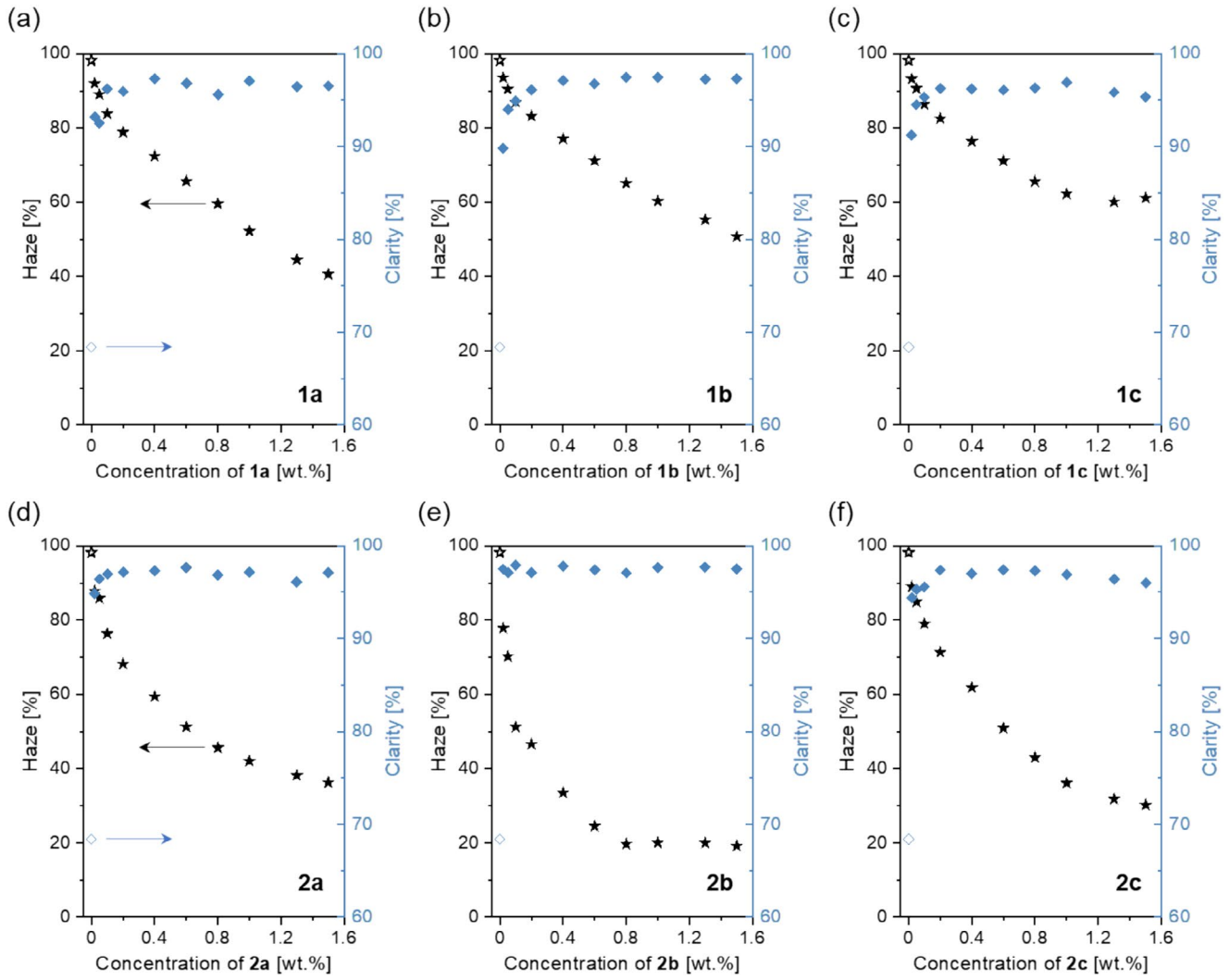

FIGURE 7 | Haze and clarity of 1.1-mm thick specimen of neat PA6 (open symbols) and PA6 with different concentrations of bisurea compounds (filled symbols). Top row (a–c): Bisurea compounds with linear aliphatic substituents (1a–c). Bottom row (d–f): Bisurea compounds with branched aliphatic substituents (2a–c).

FIGURE 8 | Photograph of injection molded specimens of neat PA6 (left), PA6 with 0.05 wt.% of 2b (center), and PA6 with 1.0 wt.% of 2b (right), with the latter in the plateau regime of the haze. The clarity increases from left to right from 68.4% to 97.1% to 97.7% as evidenced by the sharpness of the underlying text. The haze improves from left to right from 98.2% to 77.8% to 20.0% as evidenced by the increasing transparency of the specimens.

include that 2b could adopt a defective crystal structure or self-assemble into small stacks that arrange themselves between the extended polyamide chains. A switch from one polymorph to another driven by secondary interactions, here in the presence of the polyamide melt, is a possible explanation, which we recently demonstrated in the case of interactions of tailor-made bisamides with perovskites during their formation [44].

3 | Conclusion

We have demonstrated for the first time that the class of bisurea compounds, which consists of a *trans*-1,4-disubstituted cyclohexane core to which two aliphatic bisurea moieties are attached, is highly suitable as efficient nucleating and clarifying agents for the engineering plastic PA6. In particular, the reported six bisurea

additives are able to increase the peak crystallization temperature $T_{c,p}$ of PA6 from 186.5°C to more than 192°C by adding them in minute amounts of only 0.02 wt.%. Isothermal crystallization studies at different temperatures and concentrations using the bisurea compound with *tert*-butyl substituents confirm that the crystallization kinetics change significantly. The evaluation of the Avrami parameters showed that the addition of the supramolecular additive to PA6 not only leads to an increase in the nucleation rate with increasing bisurea concentration, but also changes the mechanism of nucleation and growth from three-dimensional morphology of the neat PA6 reference to a one- to two-dimensional morphology of the PA6 with the supramolecular additive.

An intriguing aspect is that the bisurea compound with the *tert*-butyl groups is able to predominantly induce the α modification of PA6. The ratio of the α phase (R_α) is increased from 57% of the neat PA6 reference to 90% of the PA6 with 1.0 wt.% of the additive. The predominated presence of the α form in combination with the smaller crystal size and the overall solid-state morphology leads to a remarkable improvement in the optical properties. We showed that for 1.1-mm thick injection molded specimens, the haze values are improved from 98% for neat PA6 to 19% for PA6 with the addition of 0.8 wt.% of the bisurea compound with the *tert*-butyl groups. Similarly, the clarity is improved from 68% to 97%.

These results demonstrate that the class of *trans*-1,4-cyclohexane bisurea compounds is capable of efficiently nucleating and clarifying PA6, resulting in specimens of PA6 with high clarity and low haze by fast standard processing methods such as injection molding, which could not be achieved before. First results indicate that this class of supramolecular additives can be used to nucleate and clarify other aliphatic semicrystalline polyamides such as PA66, PA12, and related copolyamides.

4 | Experimental Section

4.1 | Materials

Details on the synthesis and characterization of bisurea compounds 1a–c and 2a–c are given in the Supporting Information, Sections S1 and S2. As PA6 grade, Ultramid B27E was used, which was provided by BASF SE.

4.2 | Masterbatch Preparation

PA6 pellets were ground in a ZM200 freezer mill (Retsch, Haan, Germany) using a mesh size of 1000 μm at a rotation speed of 18,000 rpm. The ground PA6 powder was dried at 100°C for 12 h. The polyamide powder was mixed with 1.5 wt.% of the finely powdered corresponding bisurea compound. A self-made tumble mixer was used to achieve a homogeneous powder–powder mixture of the polyamide powder and the bisurea compound at 40–45 rpm for 24 h.

4.3 | Compounding and Preparation of Injection Molded Specimen

Compounding was performed using a twin-screw microcompounder, Xplore 15 mL (DSM, Heerlen, The Netherlands) under nitrogen atmosphere. As compounding conditions, a melt temperature of 250°C, a residence time of 5 min, and a rotational speed of 50 rpm were selected. Different concentrations of 1.5, 1.3, 1.0, 0.8, 0.6, 0.4, 0.2, 0.1, 0.05, and 0.02 wt.% of the bisurea compound in polyamide were achieved by preparing a dilution series. For this, 14.0 g of the masterbatch with a concentration of 1.5 wt.% of the bisurea compound was compounded first. About 5.4 g of the molten polymer–bisurea mixture remained in the compounder after depletion, which was subsequently diluted to the selected concentration by adding a respective amount of neat polyamide powder. Injection molding was performed using a microinjection molding machine, Xplore 12 mL (DSM, Heerlen, The Netherlands). The barrel temperature of the injection molding unit was set to 250°C, and an injection pressure of 6 bar was used. The molten compounded mixtures were transferred from the compounder to the microinjection molding machine and subsequently injected into a polished mold for the duration of 20 s, yielding round platelets with a diameter of 25 mm and a thickness of 1.1 mm. Neat PA6 was treated in the same way to obtain a reference sample.

4.4 | Nonisothermal Characterization of Compounded Specimens

Differential scanning calorimetry (DSC) measurements to determine peak crystallization temperatures were performed with a Mettler Toledo DSC/SDTA 821e under nitrogen at a flow rate of 20 mL min^{-1}. Unless otherwise stated, two heating and cooling cycles were performed between 30°C and 250°C with heating and cooling rates of 10 K min^{-1}. To erase the thermal history, samples were held at 250°C for 5 min before each cooling run. The respective peak crystallization temperature ($T_{c,p}$) was determined at the exothermic peak minimum of the second cooling scan.

4.5 | Isothermal Characterization of Compounded Specimens

Isothermal measurements were conducted using an automated Mettler Toledo DSC 3, operated under nitrogen atmosphere at a flow rate of 20 mL min^{-1}. The polymer samples were heated from 50°C to 280°C with a heating rate of 50 K min^{-1} and held there for 15 min to ensure complete melting of residual polymer crystals. Afterward, the polymer samples were cooled quickly at a cooling rate of 50 K min^{-1} to a designated crystallization temperature and held there for 30–60 min to ensure complete crystallization. Isothermal crystallization temperatures were selected in the range of 199°C–206°C for neat PA6, 202°C–208°C for PA6 with 0.02 and PA6 with 0.4 wt.% of 2b, and 205°C–210°C for PA6 with 1.0 wt.% of **2b**. The determination of half-time crystallization times as well as the performance of the Avrami fits were performed with Origin 2015.

4.6 | Polarized Optical Microscopy

Polarized optical microscopy was performed using a DIAPHOT 300 optical microscope from Nikon equipped with a FP82HT hot stage from Mettler Toledo. Optical micrographs were recorded by a Nikon ACT-2 software using a Nikon DS Ri-2 digital camera. The crystallization morphology was determined by melting a polymer

sample under nitrogen atmosphere between two Menzel microscope slides at a temperature of 270°C for 10 min and subsequently cooling to 205°C with a cooling rate of 10 K min^{-1}. The polymer sample was kept at this temperature until isothermal crystallization was completed.

4.7 | Wide Angle X-Ray Scattering

WAXS measurements on PA6 with and without 2b were determined on injection molded specimens with a thickness of 1.1 mm. Measurements were performed with a BrukerD8 Advance X-ray diffractometer using CuKα radiation ($\lambda = 1.54$ Å). Data were recorded in the range of 10°–30° (2θ) with a step size of 0.05° and a step time of 10 s. The crystalline peak and the amorphous halo were separated according to a method described by Murthy et al. [42]. using amorphous templates with Origin2015 software. Lorentzian fits were used for the modeling of the crystalline peaks and the amorphous halo and the deconvolution of the XRD curves. The 2θ values for the peak positions were estimated to be 20.3° ± 0.1° (α_1), 23.8° ± 0.3° (α_2), 21.5° ± 0.5° (amorphous halo), and 21.3° ± 0.2° (γ_1). A FWMH value of 6.1 ± 0.5 of the amorphous halo was determined with the help of the template method by Murthy et al. [42] and was used for the modeling of the amorphous halo in the XRD curves. The total content of the crystalline α phase (C_α) was determined with Equation (3) and of the crystalline γ phase (C_γ) with Equation (4). The sum of both, as shown in Equation (5), gave the total crystallinity (C_{total}). The ratio of the α phase (R_α) was calculated with Equation 6 and the ratio of the γ phase (R_γ) with Equation (7).

$$C_\alpha(\%) = \frac{\sum A_\alpha}{\sum (A_\alpha + A_\gamma) + A_{amorph}} \tag{4}$$

$$C_\gamma(\%) = \frac{\sum A_\gamma}{\sum (A_\alpha + A_\gamma) + A_{amorph}} \tag{5}$$

$$C_{total}(\%) = C_\alpha(\%) + C_\gamma(\%) \tag{6}$$

$$R_\alpha(\%) = \frac{C_\alpha(\%)}{(C_\alpha(\%) + C_\gamma(\%))} \tag{7}$$

$$R_\gamma(\%) = \frac{C_\gamma(\%)}{(C_\alpha(\%) + C_\gamma(\%))} \tag{8}$$

4.8 | Optical Characterization—Haze and Clarity

Haze and clarity values were determined according to ASTM D-1003 on injection molded platelets using a Haze-Gard Plus instrument (BYK Gardner GmbH, Germany). All optical data were measured 24 h after specimen preparation. All values given are the arithmetic average of at least three measured specimens.

Acknowledgments

Financial support from BASF SE (Ludwigshafen) and the University of Bayreuth is gratefully acknowledged. We are grateful to Prof. Paul Smith (ETH Zürich) for many fruitful and stimulating discussions. We are deeply thankful for his profound advice and for sharing his knowledge not only for this project but on many occasions. We also appreciate Arnold Schneller and Claus Gabriel (BASF SE) for fruitful discussions. The authors thank the Keylab Small Scale Processing of the Bavarian Polymer Institute for providing access to the facilities and Dr. Reiner Giesa for his support. Jutta Failner and Sandra Opel (Macromolecular Chemistry I) are gratefully acknowledged for their help in the synthesis and characterization of the bisurea compounds.

References

1. M. I. Kohan, ed., *Nylon Plastics Handbook* (Hanser, 1995).

2. R. Rulkens and C. Koning, *Polymer Science. A Comprehensive Reference*, ed. K. Matyjaszewski and M. Möller (Elsevier Science & Technology, 2012), 431–467.

3. K. Bernland, J. G. P. Goossens, P. Smith, and T. A. Tervoort, "On Clarification of Haze in Polypropylene," *Journal of Polymer Science Part B: Polymer Physics* 54 (2016): 865–874.

4. J. Molnár, Ö. Sepsi, G. Erdei, S. Lenk, F. Ujhelyi, and A. Menyhárd, "Modeling of Light Scattering and Haze in Semicrystalline Polymers," *Journal of Polymer Science* 58 (2020): 1787–1795.

5. H. Arimoto, M. Ishibashi, M. Hirai, and Y. Chatani, "Crystal Structure of the γ-Form of Nylon 6," *Journal of Polymer Science. Part A, Polymer Chemistry* 3 (1965): 317.

6. D. R. Holmes, C. W. Bunn, and D. J. Smith, "The Crystal Structure of Polycaproamide: Nylon 6," *Journal of Polymer Science* 17 (1955): 159–177.

7. S. Dasgupta, W. B. Hammond, and W. A. Goddard, "Crystal Structures and Properties of Nylon Polymers From Theory," *Journal of the American Chemical Society* 118 (1996): 12291–12301.

8. Y. Li and W. A. Goddard, "Nylon 6 Crystal Structures, Folds, and Lamellae From Theory," *Macromolecules* 35 (2002): 8440–8455.

9. G. Rotter and H. Ishida, "FTIR Separation of Nylon-6 Chain Conformations: Clarification of the Mesomorphous and γ-Crystalline Phases," *Journal of Polymer Science, Part B: Polymer Physics* 30 (1992): 489.

10. T. D. Fornes and D. R. Paul, "Crystallization Behavior of Nylon 6 Nanocomposites," *Polymer* 44 (2003): 3945–3961.

11. R. Seguela, "Overview and Critical Survey of polyamide6 Structural Habits: Misconceptions and Controversies," *Journal of Polymer Science* 58 (2020): 2971–3003.

12. Y. Liu, L. Cui, F. Guan, et al., "Crystalline Morphology and Polymorphic Phase Transitions in Electrospun Nylon 6 Nanofibers," *Macromolecules* 40 (2007): 6283–6290.

13. E. Parodi, G. W. M. Peters, and L. E. Govaert, "Structure–Properties Relations for Polyamide 6, Part 1: Influence of the Thermal History During Compression Moulding on Deformation and Failure Kinetics," *Polymers* 10 (2018): 710.

14. I. Kolesov, D. Mileva, and R. Androsch, "Mechanical Behavior and Optical Transparency of Polyamide 6 of Different Morphology Formed by Variation of the Pathway of Crystallization," *Polymer Bulletin* 71 (2014): 581–593.

15. M. Kyotani and S. Mitsuhashi, "Studies on Crystalline Forms of Nylon 6. II. Crystallization From the Melt," *Journal of Polymer Science, Polymer Physics Edition* 10 (1972): 1497.

16. Y. Zhang, Y. Zhang, S. Liu, et al., "Phase Stability and Melting Behavior of the α and γ Phases of Nylon 6," *Journal of Applied Polymer Science* 120 (2011): 1885.

17. R. Androsch, M. Stolp, and H.-J. Radusch, "Crystallization of Amorphous Polyamides From the Glassy State," *Acta Polymerica* 47 (1996): 99.

18. X. Zhang, A. Gohn, G. Mendis, J. F. Buzinkai, S. J. Weigand, and A. M. Rhoades, "Probing Three Distinct Crystal Polymorphs of

Melt-Crystallized Polyamide 6 by an Integrated Fast Scanning Calorimetry Chip System," *Macromolecules* 54 (2021): 7512–7528.

19. V. Miri, S. Elkoun, F. Peurton, et al., "Crystallization Kinetics and Crystal Structure of Nylon6-Clay Nanocomposites: Combined Effects of Thermomechanical History, Clay Content, and Cooling Conditions," *Macromolecules* 41 (2008): 9234–9244.

20. M. Inoue, "Nucleating Effect on the Kinetics of Crystallization and the Spherulites of Nylon 6," *Journal of Polymer Science Part A: General Papers* 1 (1963): 2013.

21. C.-H. Chen, H.-Y. Li, C.-Y. Chien, F.-S. Yen, H.-Y. Chen, and J.-M. Lin, "Preparation and Characterization of α-Al_2O_3/Nylon 6 Nanocomposite Masterbatches," *Journal of Applied Polymer Science* 112 (2009): 1063–1069.

22. D. G. Martínez-Vázquez, F. J. Medellín-Rodríguez, P. J. Phillips, and S. Sanchez-Valdes, "Heterogeneous Nucleation of Nylon 6 and PET With Selected Inorganic Compounds," *Journal of Applied Polymer Science* 88 (2003): 360–368.

23. M. Avella, M. E. Errico, and G. Gentile, "Nylon 6/Calcium Carbonate Nanocomposites: Characterization and Properties," *Macromolecular Symposia* 234 (2006): 170–175.

24. A. Kiziltas, B. Nazari, D. J. Gardner, and D. W. Bousfield, "Polyamide 6-Cellulose Composites: Effect of Cellulose Composition on Melt Rheology and Crystallization Behavior," *Polymer Engineering and Science* 54 (2014): 739–746.

25. B. F. Jogi, M. Sawant, P. K. Brahmankar, D. Ratna, and M. C. Tarhekar, "Study of Mechanical and Crystalline Behavior of Polyamide 6/Hytrel/Carbon Nanotubes (CNT) Based Polymer Composites," *Procedia Materials Science* 6 (2014): 805–811.

26. C. Kaynak and S. Sankal, "Effects of Oxidative Functionalized and Aminosilanized Carbon Nanotubes on the Crystallization Behaviour of Polyamide-6 Nanocomposites," *Polymer Bulletin* 71 (2014): 855–873.

27. M. Gahleitner, C. Grein, S. Kheirandish, and J. Wolfschwenger, "Nucleation of Polypropylene Homo- and Copolymers," *International Polymer Processing* 26 (2011): 2–20.

28. M. Blomenhofer, S. Ganzleben, D. Hanft, et al., ""Designer" Nucleating Agents for Polypropylene," *Macromolecules* 38 (2005): 3688–3695.

29. M. Dobrzyńska-Mizera, M. Dutkiewicz, T. Sterzyński, and M. L. Di Lorenzo, "Polypropylene-Based Composites Containing Sorbitol-Based Nucleating Agent and Siloxane-Silsesquioxane Resin," *Journal of Applied Polymer Science* 133 (2016): 43476.

30. A. Romankiewicz, T. Sterzynski, and W. Brostow, "Structural Characterization of α- and β-Nucleated Isotactic Polypropylene," *Polymer International* 53 (2004): 2086–2091.

31. M. C. Etter, Z. Urbanczyk-Lipkowska, M. Zia-Ebrahimi, and T. W. Panunto, "Hydrogen Bond-Directed Cocrystallization and Molecular Recognition Properties of Diarylureas," *Journal of the American Chemical Society* 112 (1990): 8415–8426.

32. R. M. Versteegen, R. P. Sijbesma, and E. W. Meijer, "Synthesis and Characterization of Segmented Copoly(Ether Urea)s With Uniform Hard Segments," *Macromolecules* 38 (2005): 3176–3184.

33. M. Díaz, J. A. Palop, C. Sanmartín, and E. Lizarraga, "Thermal Stability and Decomposition of Urea, Thiourea and Selenourea Analogous Diselenide Derivatives," *Journal of Thermal Analysis and Calorimetry* 127 (2017): 1663–1674.

34. S.-P. Rwei, P. Ranganathan, and Y.-H. Lee, "Isothermal Crystallization Kinetics Study of Fully Aliphatic PA6 Copolyamides: Effect of Novel Long-Chain Polyamide Salt as a Comonomer," *Polymers* 11 (2019): 472.

35. N. Vasanthan, H. Ly, and S. Ghosh, "Impact of Nanoclay on Isothermal Cold Crystallization Kinetics and Polymorphism of Poly(L-Lactic Acid) Nanocomposites," *Journal of Physical Chemistry. B* 115 (2011): 9556–9563.

36. M. Avrami, "Kinetics of Phase Change. I General Theory," *Journal of Chemical Physics* 7 (1939): 1103–1112.

37. M. Avrami, "Kinetics of Phase Change. II Transformation-Time Relations for Random Distribution of Nuclei," *Journal of Chemical Physics* 8 (1940): 212–224.

38. A. T. Lorenzo, M. L. Arnal, J. Albuerne, and A. J. Müller, "DSC Isothermal Polymer Crystallization Kinetics Measurements and the Use of the Avrami Equation to Fit the Data: Guidelines to Avoid Common Problems," *Polymer Testing* 26 (2007): 222–231.

39. E. Piorkowska and G. C. Rutledge, *Handbook of Polymer Crystallization* (John Wiley & Sons, Inc, 2013).

40. Y. An, S. Wang, R. Li, D. Shi, Y. Gao, and L. Song, "Effect of Different Nucleating Agent on Crystallization Kinetics and Morphology of Polypropylene," *E-Polymers* 19 (2019): 32–39.

41. P. Cebe and S.-D. Hong, "Crystallization Behaviour of Poly(Ether-Ether-Ketone)," *Polymer* 27 (1986): 1183–1192.

42. N. S. Murthy and H. Minor, "Analysis of Poorly Crystallized Polymers Using Resolution Enhanced X-Ray Diffraction Scans," *Polymer* 36 (1995): 2499–2504.

43. M. Schmidt, C. S. Zehe, R. Siegel, et al., "NMR-Crystallographic Study of Two-Dimensionally Self-Assembled Cyclohexane-Based Low-Molecular-Mass Organic Compounds," *CrystEngComm* 15 (2013): 8784.

44. M. Kuhn, F. A. Wenzel, C. Greve, et al., "Tailored Supramolecular Additives to Control the Crystallization Process and Morphology of MAPbI3," *Small* 21 (2025): e2410230.

Supporting Information

Additional supporting information can be found online in the Supporting Information section.